From Waste to Waste: Iron Blast Furnace Slag for Heavy Metal Ions Removal from Aqueous System

Sabah M. Abdelbasir (sfoda20@hotmail.com)
CMRDI https://orcid.org/0000-0003-2698-2041
Mohamed A. Abdel Khalek
Central Metallurgical Research and Development Institute

Research Article

Keywords: Blast furnace slag, Removal; Adsorption, Heavy metals, Kinetics, Industrial wastewater

Posted Date: January 7th, 2022

DOI: https://doi.org/10.21203/rs.3.rs-1154692/v1

Version of Record: A version of this preprint was published at Environmental Science and Pollution Research on March 31st, 2022. See the published version at https://doi.org/10.1007/s11356-022-19834-3.

Abstract

Blast furnace slag (BFS) is considered a cheap sorbent for the get rid of Co^{2+} and Pb^{2+} ions from an aqueous medium. The slag is characterized using X-ray diffraction (XRD), X-ray fluorescence (XRF), N_2 adsorption-desorption isotherms, energy dispersive X-ray analysis (EDX), scanning electron microscopy (SEM), and zeta potential. The removal of Co^{2+} and Pb^{2+} ions was carried out using batch adsorption experiments from an aqueous medium. The influence of several variables as pH, duration, sorbent quantity, temperature, and preliminary ions concentration was considered. The isotherm, kinetic, thermodynamic, and recyclability were also conducted. The maximum uptake capacity for Co^{2+} and Pb^{2+} was 43.8 and 30.2 mg g^{-1} achieved at pH 6 after 60 min. contact duration. The adsorption kinetics and isotherms of BFS for Co^{2+} and Pb^{2+} fitted well to Avrami and Freundlich models, respectively. The main sorption mechanism between BFS and the metal ions was ion exchange. The regeneration of the used slag was studied for reuse many cycles. In terms of economics and scalability, the treatment with the unmodified BFS has great potentials.

1. Introduction

Noxious heavy metals generated by a variety of manufacturing practices can cause significant environmental harm if not efficiently eliminated from the waste discharges (Sall et al. 2020). These heavy metals adversely affect human health, the environment, and aquatic systems when they accumulate in living creatures at levels above the permitted limits (Fu and Wang 2011; Gupta et al. 2012; Ihsanullah et al. 2016). Among the heavy metal ions, Pb^{2+} and Co^{2+} represent a greater hazard to human health. Acute Pb^{2+} exposure, for example, can result in newborn brain harm as well as nervous system, kidney, and vascular system disorders (Fathy et al. 2021). Generally, when Pb^{2+} ions compile in living cells, they interact with the proteins' sulfhydryl group disrupting many biological and metabolic activities (Wang et al. 2016). Cobalt noxiousness can induce asthma symptoms as well as liver, thyroid, and heart problems. At high concentrations, it can also cause genetic changes in living creatures (Jaishankar et al. 2014; Sall et al. 2020; Briffa et al. 2020). Furthermore, these two metal ions are recognized as potential cancer-causing agents, and they have been used as model contaminants for adsorption researches despite their toxicity (Khulbe and Matsuura 2018; Abdelbasir et al. 2021).

Eliminating these metals from polluted water is critical for both human health and environmental conservation. Metals are traditionally precipitated by adding hydroxyl or sulfate agents. Nevertheless, those techniques yield significant quantities of hazardous byproducts and are ineffective for negligible metals concentrations (Bazrafshan et al. 2015). For these waters having low metal concentrations, activated carbon adsorption, ion exchange, and membrane technology are effective management options (Alafif et al. 2019). However, the considerable expense and need for pretreatment are disadvantages of these methods. As a result, a frequently recommended practice for the elimination of heavy metal ions from waste discharges has been the use of economically affordable adsorbents (Saleem et al. 2019). Such materials comprise, for instance, widely accessible raw materials and wasted industrial byproducts. Natural polymers and zeolites, clay minerals, peat, ash, and slag are the most commonly investigated affordable adsorbents (Carvalho et al. 2011). Notwithstanding its extensive application, the adsorption practice has its own constraints. The most

difficult task is the advancement of a sorbent material that is fit for a concurrent and efficient getting rid of contaminants from wastewater at ultra-low levels (Sen Gupta and Bhattacharyya 2014).

Blast furnace slag (BFS) is produced in huge quantities by iron and steel companies, pose large a major disposal challenge. In 2013, global steel slag output was approximated to be between 170 and 250 million tonnes (Gomes et al. 2018). BFS is a non-metallic output of steel manufacturing. Blast furnaces run at temperatures about 2000°C and are supplied with regulated mixtures of iron ore (Fe_2O_3 + SiO_2), coke (C), and limestone ($CaCO_3$). Steel and slag are the end products (Medina et al. 2020). Even though the majority of the slag has been disposed of as junk, it has found uses in building and soil improvement. Because BFS retrieved at high temperatures, the metals present are firmly bound to its matrix and do not easily leach, making it environmentally safe (Kanel et al. 2006). Furthermore, BFS has a high uptake capacity for heavy metals due to the existence of Si and Fe oxides and due to its availability and chemical composition, it can be used as an adsorbent for metals (Liu et al. 2010; Beh et al. 2012; Ahmed and Ahmaruzzaman 2016), phosphate (Xiong et al. 2008; Han et al. 2016), and dyes (Xue et al. 2009; Gao et al. 2017). It can be also used as Fenton-like catalytic agents to break down various organic contaminants (Arzate-Salgado et al. 2016; Nasuha et al. 2016; Cheng et al. 2017). Slag has been converted to calcium silicate hydrate to remove Pb^{2+}, Zn^{2+}, and Cu^{2+} from wastewater (Yang et al. 2019), and to tobermorite to remove Sr^{2+} and Cs^{+} (Tsutsumi et al. 2014). To adsorb Co^{2+} ions from aqueous solution, it was also converted into Slag-Oxalate composite (Le et al. 2021). NaOH was used to activate BFS, which was then used to remove Ni^{2+} from aqueous solutions (Sundhararasu et al. 2021). The post-grafting method was used to modify BFS with γ-aminopropyltriethoxysilane (APTES) to improve its adsorption performance (Wang et al. 2021).

The target of our work was to look into the use of unmodified BFS for the elimination of cobalt and lead ions by adsorption. To evaluate the performance, batch experiments were carried out. The initial concentration, pH, adsorbent dose, contact duration, and temperature were considered. The relating adsorption isotherms, kinetics, and thermodynamics were thoroughly studied. The findings of this study will have a major impact on the use of low-cost adsorbents to treat wastewater.

2. Experimental

2.1. Materials

A 5 kg sample of iron slag was obtained as a byproduct from the Egyptian Iron and Steel Co., Tabbin, Egypt. It was firstly rinsed with pure water for surface impurities removal then dried out at 105°C for a whole night. It was ground and classified according to particle size. The sample was endured to a size reduction by means of a rotating ball mill with nineteen steel balls weighing 540 g each; the longer the grinding time (almost 2 hours), the finer and non-agglomerated the particles became.

Nitrate salts of cobalt [$Co(NO_3)_2$] and lead [$Pb(NO_3)_2$] (pure Sigma-Aldrich and Merck grade) were utilized for the preparation of Co^{2+} and Pb^{2+} stock solutions using ultrapure water. Standard solutions of NaOH and HCl (0.1 mol L^{-1}) were applied for pH monitoring.

2.2. Characterization

Chemical composition and full characterization of BFS were determined using different characterization tools (**see supplemental file for full details**). The chemical composition of the BFS was detected as metal oxides. The concentration of Co^{2+} and Pb^{2+} ions was determined by atomic absorption spectroscopy (GBC-908136 AA, Australia) (Limiju, 2017).

2.3. Adsorption experiments

The characterized slag was applied as an adsorbent for Co^{2+} and Pb^{2+} ions. Adsorption experimentations were executed using 0.05 g of slag powder in 30 ml of ions solution of desired concentration, temperature, and pH in a 50 ml round bottom bottle. The bottle was shaken in a water bath at 200 rpm for a certain duration. Then, the solid sorbent is removed using a centrifuge. The residual ions were analyzed by AAS (atomic absorption spectrophotometer).

The quantity of sorbed ions per unit weight of slag, q (mg/g), is determined from the subsequent relation (Maged et al. 2020):

$$\text{Adsorption capacity "}q\text{" (mg/g)} = \frac{(\mathrm{Ci} - \mathrm{Cf}) \times \mathrm{V}}{\mathrm{W}} \quad (1)$$

The percent removal of ions was estimated from the subsequent relation (Abdelbasir et al. 2021):

$$\text{Removal efficiency \%} = \frac{C_i - C_f}{C_i} \cdot 100 \quad (2)$$

Applying that: V is the solution volume in liter (30 ml = 0.03 liter), W is the slag weight (g), C_i and C_f are the original and final ions' concentrations (mg L^{-1}).

2.4. Regeneration and desorption study

To lower the expenses of the sorption practice and recover the contaminant removed from the waste effluent, the regeneration of the adsorbent is a necessity. A 0.1 mol L^{-1} HNO_3 solution was used to study the desorption of the sorbed ions at 60°C for 30 min. (1: 10 solid-liquid ratio). AAS was used to measure the ions concentration preceding to and following desorption experiments. Equation (3) was used to calculate the desorption efficacy:

$$R_{des} = \frac{D_{des}}{A_{ads}} \; x \; 100 \quad (3)$$

The quantities of adsorbed and desorbed metal ions are represented by A_{ads} and D_{des}, correspondingly. Reusability was achieved by utilizing the regenerated adsorbent in subsequent adsorption experiments and repeating the adsorption-desorption method with the same adsorbent sample.

3. Results And Discussion

3.1. Slag characterization

The XRF analysis of BFS was achieved after grinding and the elemental composition is shown in Table 1. The average content of Ca as oxide (CaO) was approximately 46.62%, as the main element of BFS, followed by Si, Ba, Mn, and Mg. The values represent an average duplicate of BFS analysis.

Table 1

Element	Na	Zn	Mg	Si	S	K	Ca	Ti	Mn	Fe	Ba	Others
Wt. % as oxide	0.80	0.14	2.93	23.7	2.02	1.02	46.62	1.08	8.88	0.93	11.15	0.88

The particle size analysis of the slag is shown in Fig. 1**(b)** It is seen that about 50% of the sample has a particle size less than 0.90 mm, while a 90% weight of the sample is less than 0.43 mm. Also, about 80% of the sample has a particle size range from 1.16 – 0.417 mm. The degree to which finer particles are reduced is widely known to be subordinate to the material type, the mill, and the grinding circumstance (Petrakis and Komnitsas 2019) s.

Figure 1**(c)** Depicts the XRD framework of BFS. The pattern is quite intricate which is mostly due to the raw material nature. The sample is possibly amorphous glassy having a hump at about 2θ: 28˚- 33˚ (Mostafa et al. 2001). It is also worth mentioning that quite a few peaks were found indicating the presence of crystal phases in the slag.

SEM and EDX were utilized to define the size and basic structure of the BFS as displayed in Fig. 2. SEM images revealed the coarse, slack, and porous surface textures of the BFS sample (Fig. 2a **& b**). Slag particles had become angular in form, with definite asperities and edges evident. Rough surface textures were also a feature of them. The EDX analysis revealed high-intensity peaks for Ca, O, Si, Al, Mg, and other noticeable ones for Na, Ti, and S, in conformity with the analysis and XRD outcomes. Steel slags are known to include oxides, which are produced during the steelmaking process.

CaO is the most common oxide found in steel slags generated during diverse steelmaking processes (Yildirim and Prezzi 2011). In our case, FeO is one more oxide generated during some steelmaking practices with a low occurrence. Slag leachates are also frequently found to be extremely basic because of CaO and further basic oxides (Riley and Mayes 2015).

The surface area and the pore structure of BFS were assessed by the nitrogen isotherms analysis shown in Fig. 3**(a).** As we can see from the figure, the shape of the isotherm is classified as Type II, indicating that the slag with a heterogeneous granular aspect established the slit aperture shaped by the particles' accumulation (Deng et al. 2020). The specific surface, pore-volume, and average diameter of BFS are revealed in **Table S1** in the supplemental file.

Figure 3**(b)** shows the surface charge results of the slag in an electrolyte solution. The slag surface charge is clearly pH-dependent, being positively at pH less than 4.8, and becoming negatively charged as the solution

pH progressed to neutral and basic regions. A pH 4.8. was found to be the isoelectric point (IEP).

3.2. Adsorption Experiments

Adsorption batch experimentations were applied to validate the heavy metal removal efficiency using BFS as adsorbent for Pb^{2+} and Co^{2+} ions from the prepared solutions.

3.2.1. Impact of pH

The sorption procedure is greatly impacted by the medium's pH. Fig. 4**(a)** shows the removal proficiency and uptake capacity of different ions from synthetic solution. The maximum sorption capacities and removal efficiency are accomplished at pH 6. Metal ions solubility reduces at alkaline pH, enabling precipitation and complicating sorption (He et al. 2015). The concentration of external H^+ rose at low pH levels which are considered as competitive in ion exchange (Akhigbe et al. 2015; Kozera-Sucharda et al. 2020). The slag selectivity follows the order of $Co^{2+} > Pb^{2+}$. The charge density (charge/ionic radius), hydration energy, and proportions of the hydrated ions may all be used to predict the solid's vantage for various ions all through competitive sorption (**see Table S2 in the supplementary file**). Other factors, such as the geometry and/or orientation of the ions, also influence selectivity. As well, the distribution of the surface charge on slag can change based on its composition and activation. As a result, solution pH has a significant impact on the adsorbent's functional group activity. The slag surface charge is negative at a pH higher than 4.8 (Dimirkou 2007; Acheampong et al. 2010; Elboughdiri 2020). The distinct ability to adsorb ions is due to the slag's containment (Wang et al. 2021).

3.2.2. Impact of sorbent dosage

Figure 4**(b)** validates the action of the slag dose (g L^{-1}) on the elimination proficiency and uptake capability of the slag. The amount of added slag to the aqueous solution significantly affects the adsorption process. Intensifying the dose caused an upsurge of the removal efficiency while the adsorption capacity was increased up to 1.67 g L^{-1}, and then decreased. Each metal ion is subjected to a larger unit mass of the adsorbent, which has more adsorption sites which ready to attract this ion (Mahmoud et al. 2019).

3.2.3. Impact of original metal ion concentrations and sorption isotherms

Figure 5. exhibits the preliminary ion concentration's influence on the removal efficacy and uptake capacity of the slag. The concentration of ions in an aqueous medium significantly affects the adsorption practice (Abdel-Khalek et al. 2017). Increasing the initial ion concentration increased the uptake capacity and removal proficiency. A high starting concentration indicates that more ions are accessible and hence, more ions are sorbed for a fixed sorbent's amount (Khalek et al. 2019). At a higher initial concentration, the driving forces to conquer the mass transfer barrier for ions' emigration through the medium to the sorbent solid surface upsurges. Nevertheless, each unit weight of the sorbent is exposed to a greater amount of ions steadily loading the sites until fullness (Mahmoud et al. 2019).

The adsorption isotherms are the best analysis method to describe the sorption behavior (Hałas et al. 2017). Temkin, Langmuir, and Freundlich isotherms were employed to investigate the sorption practice.

Temkin Isotherm

According to the Temkin model, the adsorption heat of sorbed species in the layer declines linearly rather than logarithmically as a function of temperature (Ostrovskii 1989; Ho and McKay 1998; Hoslett et al. 2020). Temkin model equation is written as (Tsai and Chen 2013):

$$q_e = B\ln A_T + B\ln C_e$$

4

Where: q_e is the adsorbed ions at equilibrium, A_T is the equilibrium constant interrelated to the maximal binding energy (L g^{-1}), B is the Temkin isotherm constant linked to the heat of adsorption (J/mol), R is the universal gas constant (8.314 J/mol/K), and T is the temperature in kelvin. By plotting q_t against ln C_e, the constants were assessed from the plot intercept and slope (Fig. 6.). A_T and B values are found in Table 2 (the computed R^2 values are 0.8476 and 0.8914).

Table 2

Isotherm	Parameter	Pb^{2+}	Co^{2+}
Temkin	R^2	0.8914	0.8476
	B	5.7920	8.1673
	A_T (L/g)	2.1557	2.5745
Langmuir	R^2	0.9655	0.8372
	b (L/mg)	0.1062	0.0986
	q_{max}(Cal.)	34.0	52.1
	q_{max} (Exp.)	30.2	43.8
Freundlich	R^2	0.9950	0.9895
	n	1.958	1.707
	K_f (mg/g)	4.293	5.631

Langmuir Isotherm

Langmuir model's equation (Chen et al. 2012) is:

$$\frac{C_f}{q_t} = \frac{C_f}{q_{max}} + \frac{1}{bq_{max}}$$

5

Knowing that C_f (mg L^{-1}) is the final ions concentration, q_t (mg g^{-1}) is the sorbed ions' amount at duration t, q_{max} (mg g^{-1}) (highest sorption) is monolayer sorption capacity and b (L mg^{-1}) is a constant associated with the sorption energy. Langmuir model adopts that the occurrence of sorption at a precise homogeneous surface of the sorbent where the ions flow through the pores and the apertures of the lattice to replenish the substitutable ions of the sorbent. From Fig. 6 and Table 3, the regression (R^2) value of Langmuir model linear fitting 0.8372 and 0.9655.

Table 3

Initial conc., mg L^{-1}	R_L	
	Pb^{2+}	Co^{2+}
5	0.9888	0.9896
10	0.4850	0.5035
25	0.2736	0.2886
50	0.1585	0.1686
75	0.1115	0.1191
100	0.0861	0.0921

Freundlich Isotherm

This isotherm model(Visa 2016) equation could be written as:

$$lnq_t = lnK_f + \frac{1}{n} lnC_f$$

6

Where K_f (Freundlich constant, mg/g), is the connotative of the degree of the sorption and n is the sorption intensity.

K_f points to the uptake capacity, whereas 1/n is a function of the sorption capability (Tsai and Chen 2013; Shehab et al. 2019). If n = 1, the barrier between the two phases is unaffected by concentration. If n is less than 1, it assigns typical adsorption and if it lies between 1 and 10, a favorable sorption process is nominated (Goldberg 2018). From Table 2, the values of n are 1.707 and 1.958 while R^2 values are 0.9895 and 0.995 indicating that the sorption procedure is favorable and of physical character (Abdel-Khalek et al. 2020).

The dimensionless equilibrium parameter or separation factor (R_L):

It is assigned as:

$$R_L = \frac{1}{(1 + bC_0)}$$

7

Implying that, C_0 (mg L^{-1}) is the starting metal ions' concentration and b is Langmuir's constant. R_L value specifies whether the sorption is advantageous or non-advantageous. If R_L values lie between 0 and 1 then, the sorption procedure is auspicious, whereas R_L = 1 denotes non-advantageous linear sorption, and R_L = 0 signifies non-reversible sorption.

The results showed that the value of R_L is almost unity with 5 mg L^{-1} which indicates unfavorable adsorption. While at other concentrations up to 100 mg L^{-1}, R_L is between 0 and 1 designating advantageous adsorption.

3.2.4. Time Impact and Sorption kinetics

To find an appropriate contact time for the adsorption, the uptake capacity and removal efficiency of various ions were evaluated as a function of time, Fig. 7. The equilibrium time was determined to be 60 minutes. The increased sorption rate at the early 20 minutes is owing to the accessibility of ions and vacant sorption spots on the slag's surface. Then, the sorption active spots steadily lessened, and the extent of sorption was assessed by the number of ions transferred from the solution to the sorption active spots. Thus, the sorption increases with time until fullness is reached (Zare et al. 2018; Abdel-Khalek et al. 2020). Also, the ions required more time to infiltrate the tiny pores. The higher initial rate implies that the adsorption happens on the exterior surface first, ensued by the interior pores. Furthermore, the larger adsorption quantity in the first period demonstrated higher sorption on the exterior surface rather than in the pores (Zare et al. 2016).

The sorption extent of metal ions by the slag was examined via the Lagergren pseudo-first-order and pseudo-second-order models. Also, the Avrami model was used which describes a fractional kinetic order (Lopes et al. 2003; Issaoui et al. 2021). The Lagergren for the pseudo-first-order (PFO) and pseudo-second-order (PSO) models were denoted as shown in the coming equations:

PFO model $\ln(q_e\text{-}q_t) = \ln q_e - K_1 t$ (8)

PSO model $t/q_t = 1/K_2 q_e^2 - t/q_e$ (9)

Where k_1 (min^{-1}) and k_2 (g $mg^{-1}.min^{-1}$) are the equilibrium rate constants.

The Avrami model was expressed as follows (He and Duan 2016; Narayanan et al. 2020):

$$\ln[-ln(1-)] = n\ln K_{avr} + n\ln t$$

10

The model explains a system with a time-dependent rate coefficient. It provides the greatest fitting of metal ion intake on sorbents (Issaoui et al., 2021; Vaghetti et al., 2009). The integral form is where K is the Avrami constant, and n is a constant interrelated to the sorption mechanism.

$$Q_t = Q_m - Q_m e^{-K_{avr}.t^n}$$

11

$$\frac{Q_t}{Q_m} = 1 - e^{-K_{avr}.\, t^n}$$

12

The $\frac{Q_t}{Q_m}$ is the adsorption fraction "α". By plotting "$\ln[-ln(1-)]$" versus "ln t", the **n** and **K** can be computed from the intercept and slope as follow: the slope equal "**n**" and the intercept equals "**n ln K**".

The acquired outcomes of the three linearized models are displayed in Fig. 8 besides, their equivalent limits are listed in Table 4. Even though the PFO and PSO models are the most widely applied that forecast closer values of the equilibrium uptake capacity, the best-fitting was found using Avrami's linear retrogression, based on R^2 closest value to unity. The kinetic fitting quality changes in the subsequent order: Avrami > PSO > PFO. The Avrami model has value of R^2 (> 0.98).

Table 4

Model	Item	Pb^{2+}	Co^{2+}
1st order	R^2	0.9389	0.9244
	K_1	-0.0614	-0.0637
	q_{max} cal.	20.4	21.6
	q_{max} exp.	19.3	23.5
2nd order	R^2	0.9736	0.9792
	K_2	0.0032	0.0043
	q_{max} cal.	22.2	25.7
	q_{max} exp.	19.3	23.5
Avrami	R^2	0.9895	0.9836
	n	1.1797	1.1882
	K	0.0580	0.0759

Another kinetic model, reliant on chemical sorption, is the particle diffusion model. It entails the replacing or sharing electrons between the sorbent and metal ions (Jiang et al. 2010). It is assumed that adsorption occurs due to the flow of metal ions from the liquid to the sorbent exterior surface, ensued by ions dispersal into the pores. It is a time-consuming process that is proportional to $time^{0.5}$ denoted as (Covelo et al. 2007):

$$q_t = k_{id} t^{0.5} + I$$

13

q_t is the amount of sorbed ions after contact duration t where $t^{0.5}$ is its square root and K_{id} (mg g^{-1} $min^{-0.5}$) is the rate constant and I is the intercept whose values provide statistics about the boundary layer's depth, i.e., the bigger the intercept the larger the influence of that borderline layer is.

Figure 9 and Table 5 show that the diffusion represents a restraining phase in the operations on the sorbent. The increased adsorption capacity confirms the presence of mesopores, with a significant amount of sites, unlocked for the small ions. However, the linear plot of $t^{0.5}$ against q_t, fit data with good linear regression coefficients ($R^2 \approx 0.91$). It indicates the applicability of the model and the rate-monitoring step is intra-particle diffusion (Goldberg 2018).

Table 5

Parameter	Pb^{2+}	Co^{2+}
linear regression coefficients (R^2)	0.9106	0.9098
Thickness of boundary layer (I)	2.8206	5.4130
Rate constant of intra-particle diffusion (K_{id})	1.8917	2.1189

3.2.5. Temperature Impact and Sorption Thermodynamics

Figure 10 displays the influence of temperature on the sorption practice. The extreme uptake capacity was reached at 65°C, signifying that the sorption is an endothermic process. Most adsorption studies suggest that increasing the temperature improves the sorption process (Argun 2008; Mercado-Borrayo et al. 2020; Plaza et al. 2021). Typically, at higher temperatures, the uptake is greater due to an increase in the energetic spots of the sorbent material. At increased temperatures, the system's energy promotes the ions' attachment to the mineral's surface (Arief et al. 2008). Also, the movement of the ions becomes faster due to decreasing the viscosity of the solution (Fakari and Nezamzadeh-Ejhieh 2017), resulting in higher removal efficiencies (Rukayat et al. 2021).

Changes in thermodynamics parameters such as Gibb's free energy (ΔG°), entropy (ΔS°), and enthalpy (ΔH°) (Plaza et al. 2021) were determined. ΔH° and ΔS° were computed from Van't Hoff equation (Karmaker et al. 2019):

$$\ln K_c = \frac{\Delta S^\circ}{R} - \frac{\Delta H^\circ}{RT}$$

14

Where kc = F/(1 − F), and F = (C_0 − Ce)/C_0, R is the universal gas constant, and T is the temperature in K. The relationship of ln kc versus 1/T (Fig. 11.) gives a straight line with a slope of −ΔH°/R and an intercept equals to ΔS°/R. The positive values of ΔH° in Table 6 specified the endothermic sorption process. Additionally, the ΔH° value < 30 kJ mol^{-1} verifies the physico-sorption process as shown by the Freundlich isotherm (Karmaker et al. 2019). Additionally, ΔS° was found to have positive values, suggesting a degree of unpredictability at the interface between the sorbent and adsorbate, inferring that sorption is less advantageous at lower temperatures.

Table 6
shows that the sorption is unprompted since the ΔG° has negative values. It should be pointed out here that as the temperature rose, so did the negative values of ΔG°, suggesting that sorption is more favorable at higher temperatures (Ghasemi et al. 2020; Hassan et al. 2020).

Metal ion	Temp.(°C)	ΔG°(kJ mol^{-1})	ΔH° (kJ mol^{-1})	ΔS° (J mol^{-1} k^{-1})
(Pb^{2+})	25	-1346	27.6	96.7
	35	-2092		
	45	-2918		
	55	-4032		
	65	-5253		
(Co^{2+})	25	-3052	24.6	92.2
	35	-3719		
	45	-4528		
	55	-5586		
	65	-6772		

ΔG° is estimated via the subsequent relation (Hoang et al. 2019) :

$$\Delta G^\circ = -RTlnK_c$$

15

3.2.6. Adsorption mechanism

As revealed by isotherm studies, the adsorption process fits the Freundlich isotherm thus obeying multilayer sorption of Pb^{2+} and Co^{2+} on BFS (physical adsorption). Inner layer sorption of metal ions on BFS might be ascribed to the creation of metal-Si complex between the Pb^{2+}/Co^{2+} ion and Si of the slag via the exchange of H^+ ions in the circumference. Moreover, the negatively charged BFS surface (at pH 6) favors the electrostatic interaction with positive metal ions.

As a result, the electrostatic interaction between Pb^{2+}/Co^{2+} ions and the groups (suchlike $-CO_3$ and $-OH$) on the sorbent is linked with multilayer adsorption of metal ions. Metal-sulfur complex formation via ion exchange and electrostatic interactions is thought to be a viable mechanistic mechanism for metal-ion adsorption on the BFS. Considering the nature and composition of the BFS, an exchange interaction of the slag with the effluent may be described as coming (Dimitrova and Mehandgiev 1998):

$$\text{-SiO (Ca)} + 2\text{H-OH} \rightarrow \text{-Si-O-H}_2 + Ca^{2+} + 2(\text{-}OH^-) \quad (16)$$

It can be anticipated that because of the large concentration of hydrogen ions in an acidic environment, the above reaction should shift to the left side. Following the aforesaid approach, the basic slags had a neutralizing impact.

Undoubtedly, Ca^{2+} ions interacted with the freed H^+ ions from the slag when the solution pH rose, confirming the occurrence of the reaction in Eq. (17) when the BFS came in contact with solutions. The BFS slag exhibited a strong ion exchange capacity, which was consistent with the sorption equilibrium. For divalent metal ions (M^{2+}) in solutions, the aforementioned equation may be expressed as (Zhan et al. 2019):

$$(\text{Si-}O^-)_2Ca^{2+} + H_3O^+ \rightarrow 2(\text{Si-OH}) + Ca^{2+} + OH^- \quad (17)$$

The lone pair of electrons in the oxygen atoms of OH^- groups play an important role in the complexation between metal ions and these OH^- groups (Wang et al. 2021)

For Pb^{2+}

$$(\text{Si-}O^-)_2Ca^{2+} + 2\text{Pb-}OH^+ \rightarrow 2\text{Si-O-PbOH} + Ca^{2+} \quad (18)$$

$$\text{Si-}O^- + \text{HOH} + PbOH^+ \rightarrow \text{Si-O-PbOH} + H_3O^+ \quad (19)$$

For Co^{2+}

$$(\text{Si-}O^-)_2Ca^{2+} + 2CoOH^+ \rightarrow 2\text{Si-O-CoOH} + Ca^{2+} \quad (20)$$

$$\text{Si-}O^- + \text{HOH} + CoOH^+ \rightarrow \text{Si-O-CoOH} + H_3O^+ \quad (21)$$

3.2.7. Regeneration and desorption

The regeneration and reusability of the slag for Co^{2+} and Pb^{2+} ions removal was examined under the maximum adsorption conditions: 50 mg L^{-1} initial ions concentration; 3.3 g L^{-1} slag dose; pH 6; at 65°C and 60 min duration. Whereas the conditions for regeneration were: 0.1 M HNO_3; solid/liquid ratio of 1: 10; at 60°C for 30 minutes contact. As revealed in **Fig. S1**, the adsorbed cobalt and lead ions on the slag surface could be efficaciously desorbed with proficiency exceeding 91% for the first cycle. Additionally, the removal efficiency was reduced by a few percent in the next three cycles. These results revealed that the slag could be reused repetitively to get rid of Co^{2+} and Pb^{2+} ions from discharge effluents.

To sum up, the present study using blast furnace slag has touched on the technical merit of slags that can be used as efficient adsorbents for decontaminating waste effluents of industries. Additionally, the gained outcomes assert promisingly that the considered process may meet the requirements of using slag adsorbents at a cheap and plentiful source for large-scale production. Comparison with the other iron steel and slag adsorbents used for Pb^{2+} and Co^{2+} removal from wastewater is exhibited in **Table S3** in the supplemental file.

4. Conclusion

Blast furnace slag (BFS) has a complex composition. Its surface charge is pH-dependent, where the isoelectric point is at pH 4.8. It was successfully used, without modification, as a sorbent of heavy metal ions. The maximum removal of Co^{2+}: 43.8 and Pb^{2+}: 30.2 mg g^{-1} were achieved at pH 6, 65°C for 60 min. Its selectivity follows the order of $Co^{2+} > Pb^{2+}$ which is attributed to the hydration energy and charge density. The Freundlich isotherm model fits well indicating the physical nature of the sorption progression. The dimensionless separation factor (R_L) indicates favorable adsorption. The higher adsorption amount in the first duration verified the sorption favorability on the BFS exterior surface over that in the interior pores. The particle diffusion model describes the sorption is occurred by the ions flowing from the aqueous phase to the sorbent's exterior surface, pursued by ions dispersion into the apertures and pores. The best-fitting was attained by applying linear regression of the Avrami kinetic model.

The lower positive ΔH° designates the endothermal character which confirms the physico-sorption practice. The positive ΔS° indicates a high degree of randomness. The negative ΔG° designates spontaneity of the sorption practice. The regeneration revealed that the slag could be reused repetitively to remove cobalt and lead ions from effluents.

Declarations

Declaration of interests

No opposing financial interest to pronounce.

References

1. Abdelbasir SM, El-Shewaikh AM, El-Sheikh SM, Ali OI (2021) Novel modified chitosan nanocomposites for Co(II) ions removal from industrial wastewater. Journal of Water Process Engineering 41:102008. https://doi.org/10.1016/j.jwpe.2021.102008
2. Abdel-Khalek MA, Abdel Rahman MK, Francis AA (2017) Exploring the adsorption behavior of cationic and anionic dyes on industrial waste shells of egg. Journal of Environmental Chemical Engineering 5:319–327. https://doi.org/10.1016/j.jece.2016.11.043
3. Abdel-Khalek MA, Abdel Rahman MK, Francis AA (2020) Experimental Design and Desirability Analysis for Optimizing the Bio-sorption of Liquid Paint-related Wastes onto Solid Eggshell Wastes. Environmental Processes 7:493–508. https://doi.org/10.1007/s40710-020-00435-6

4. Acheampong MA, Meulepas RJW, Lens PNL (2010) Removal of heavymetals and cyanide from gold mine wastewater. Journal of Chemical Technology and Biotechnology 85:590–613
5. Ahmed MJK, Ahmaruzzaman M (2016) A review on potential usage of industrial waste materials for binding heavy metal ions from aqueous solutions. Journal of Water Process Engineering 10:39–47
6. Akhigbe L, Ouki S, Saroj D (2015) Removal of Escherichia coli and heavy metals from aqueous solutions using silver-modified clinoptilolite. Desalination and Water Treatment 55:777–782. https://doi.org/10.1080/19443994.2014.929980
7. Alafif ZO, Anjum M, Kumar R, et al (2019) Synthesis of CuO–GO/TiO2 visible light photocatalyst for 2-chlorophenol degradation, pretreatment of dairy wastewater and aerobic digestion. Applied Nanoscience (Switzerland) 9:579–591. https://doi.org/10.1007/s13204-018-0921-7
8. Argun ME (2008) Use of clinoptilolite for the removal of nickel ions from water: Kinetics and thermodynamics. Journal of Hazardous Materials 150:587–595. https://doi.org/10.1016/j.jhazmat.2007.05.008
9. Arief VO, Trilestari K, Sunarso J, et al (2008) Recent progress on biosorption of heavy metals from liquids using low cost biosorbents: Characterization, biosorption parameters and mechanism studies. Clean - Soil, Air, Water 36:937–962
10. Arzate-Salgado SY, Morales-Pérez AA, Solís-López M, Ramírez-Zamora RM (2016) Evaluation of metallurgical slag as a Fenton-type photocatalyst for the degradation of an emerging pollutant: Diclofenac. In: Catalysis Today. Elsevier B.V., pp 126–135
11. Bazrafshan E, Mohammadi L, Ansari-Moghaddam A, Mahvi AH (2015) Heavy metals removal from aqueous environments by electrocoagulation process - A systematic review. Journal of Environmental Health Science and Engineering 13:1–16
12. Beh CL, Chuah TG, Nourouzi MN, Choong T (2012) Removal of heavy metals from steel making waste water by using electric arc furnace slag. E-Journal of Chemistry 9:2557–2564. https://doi.org/10.1155/2012/128275
13. Briffa J, Sinagra E, Blundell R (2020) Heavy metal pollution in the environment and their toxicological effects on humans. Heliyon 6:e04691
14. Carvalho J, Araujo J, Castro F (2011) Alternative low-cost adsorbent for water and wastewater decontamination derived from eggshell waste: An overview. Waste and Biomass Valorization 2:157–167
15. Chen X, Guo Y, Cheng F, et al (2012) Application of modified coal fly ash as an absorbent for ammonia-nitrogen wastewater treatment. In: Advanced Materials Research. Trans Tech Publications Ltd, pp 2380–2384
16. Cheng M, Zeng G, Huang D, et al (2017) Salicylic acid–methanol modified steel converter slag as heterogeneous Fenton-like catalyst for enhanced degradation of alachlor. Chemical Engineering Journal 327:686–693. https://doi.org/10.1016/j.cej.2017.06.153
17. Covelo EF, Vega FA, Andrade ML (2007) Simultaneous sorption and desorption of Cd, Cr, Cu, Ni, Pb, and Zn in acid soils: I. Selectivity sequences. Journal of Hazardous Materials 147:852–861. https://doi.org/10.1016/J.JHAZMAT.2007.01.123

18. Deng M, Wang X, Li Y, et al (2020) Reduction and immobilization of Cr(VI) in aqueous solutions by blast furnace slag supported sulfidized nanoscale zerovalent iron. Science of The Total Environment 743:140722. https://doi.org/10.1016/J.SCITOTENV.2020.140722
19. Dimirkou A (2007) Uptake of Zn2+ ions by a fully iron-exchanged clinoptilolite. Case study of heavily contaminated drinking water samples. Water Research 41:2763–2773. https://doi.org/10.1016/j.watres.2007.02.045
20. Dimitrova S v., Mehandgiev DR (1998) Lead removal from aqueous solutions by granulated blast-furnace slag. Water Research 32:3289–3292. https://doi.org/10.1016/S0043-1354(98)00119-5
21. Elboughdiri N (2020) The use of natural zeolite to remove heavy metals Cu (II), Pb (II) and Cd (II), from industrial wastewater. Cogent Engineering 7:. https://doi.org/10.1080/23311916.2020.1782623
22. Fakari S, Nezamzadeh-Ejhieh A (2017) Synergistic effects of ion exchange and complexation processes in cysteine-modified clinoptilolite nanoparticles for removal of Cu(ii) from aqueous solutions in batch and continuous flow systems. New Journal of Chemistry 41:3811–3820. https://doi.org/10.1039/c7nj00075h
23. Fathy MA, Abdelbasir SM, Hassan SS, et al (2021) Mechanochemical activation for lead extraction from spent cathode ray tube. Journal of Material Cycles and Waste Management 2021 23:3 23:1090–1101. https://doi.org/10.1007/S10163-021-01198-4
24. Fu F, Wang Q (2011) Removal of heavy metal ions from wastewaters: A review. Journal of Environmental Management 92:407–418
25. Gao H, Song Z, Zhang W, et al (2017) Synthesis of highly effective absorbents with waste quenching blast furnace slag to remove Methyl Orange from aqueous solution. Journal of Environmental Sciences (China) 53:68–77. https://doi.org/10.1016/j.jes.2016.05.014
26. Ghasemi Z, Sourinejad I, Kazemian H, et al (2020) Kinetics and thermodynamic studies of Cr(VI) adsorption using environmental friendly multifunctional zeolites synthesized from coal fly ash under mild conditions. Chemical Engineering Communications 207:808–825. https://doi.org/10.1080/00986445.2019.1630389
27. Goldberg S (2018) Equations and models describing adsorption processes in soils. In: Chemical Processes in Soils. John Wiley & Sons, Ltd, pp 489–517
28. Gomes HI, Funari V, Mayes WM, et al (2018) Recovery of Al, Cr and V from steel slag by bioleaching: Batch and column experiments. Journal of Environmental Management 222:30–36. https://doi.org/10.1016/j.jenvman.2018.05.056
29. Gupta N, Kushwaha AK, Chattopadhyaya MC (2012) Adsorptive removal of Pb 2+, Co 2+ and Ni 2+ by hydroxyapatite/chitosan composite from aqueous solution. Journal of the Taiwan Institute of Chemical Engineers 43:125–131. https://doi.org/10.1016/j.jtice.2011.07.009
30. Hałas P, Kołodyńska D, Płaza A, et al (2017) Modified fly ash and zeolites as an effective adsorbent for metal ions from aqueous solution. Adsorption Science and Technology 35:519–533. https://doi.org/10.1177/0263617417700420
31. Han C, Wang Z, Yang W, et al (2016) Effects of pH on phosphorus removal capacities of basic oxygen furnace slag. Ecological Engineering 89:1–6. https://doi.org/10.1016/j.ecoleng.2016.01.004

32. Hassan ESRE, Rostom M, Farghaly FE, Abdel Khalek MA (2020) Bio-sorption for tannery effluent treatment using eggshell wastes; kinetics, isotherm and thermodynamic study. Egyptian Journal of Petroleum 29:273–278. https://doi.org/10.1016/j.ejpe.2020.10.002
33. He J, Duan C (2016) Recovery of metallic concentrations from waste printed circuit boards via reverse floatation. Waste Management. https://doi.org/10.1016/j.wasman.2016.11.019
34. He K, Chen Y, Tang Z, Hu Y (2015) Removal of heavy metal ions from aqueous solution by zeolite synthesized from fly ash. Environmental Science and Pollution Research 2015 23:3 23:2778–2788. https://doi.org/10.1007/S11356-015-5422-6
35. Ho YS, McKay G (1998) A Comparison of chemisorption kinetic models applied to pollutant removal on various sorbents. Process Safety and Environmental Protection 76:332–340. https://doi.org/10.1205/095758298529696
36. Hoang LP, Van HT, Nguyen LH, et al (2019) Removal of Cr(vi) from aqueous solution using magnetic modified biochar derived from raw corncob. New Journal of Chemistry 43:18663–18672. https://doi.org/10.1039/c9nj02661d
37. Hoslett J, Ghazal H, Mohamad N, Jouhara H (2020) Removal of methylene blue from aqueous solutions by biochar prepared from the pyrolysis of mixed municipal discarded material. Science of the Total Environment 714:. https://doi.org/10.1016/j.scitotenv.2020.136832
38. Ihsanullah, Abbas A, Al-Amer AM, et al (2016) Heavy metal removal from aqueous solution by advanced carbon nanotubes: Critical review of adsorption applications. Separation and Purification Technology 157:141–161
39. Issaoui H, Sallem F, Lafaille J, et al (2021) Biosorption of Heavy Metals from Water onto Phenolic Foams Based on Tannins and Lignin Alkaline Liquor. International Journal of Environmental Research 2021 15:2 15:369–381. https://doi.org/10.1007/S41742-021-00313-5
40. Jaishankar M, Tseten T, Anbalagan N, et al (2014) Toxicity, mechanism and health effects of some heavy metals. Interdisciplinary Toxicology 7:60–72
41. Jiang M qin, Jin X ying, Lu XQ, Chen Z liang (2010) Adsorption of Pb(II), Cd(II), Ni(II) and Cu(II) onto natural kaolinite clay. Desalination 252:33–39. https://doi.org/10.1016/j.desal.2009.11.005
42. Kanel SR, Choi H, Kim JY, et al (2006) Removal of arsenic(III) from groundwater using low-cost industrial by-products - Blast furnace slag. Water Quality Research Journal of Canada 41:130–139. https://doi.org/10.2166/wqrj.2006.015
43. Karmaker S, Sintaha F, Saha TK (2019) Kinetics, Isotherm and Thermodynamic Studies of the Adsorption of Reactive Red 239 Dye from Aqueous Solution by Chitosan 8B. Advances in Biological Chemistry 09:1–22. https://doi.org/10.4236/abc.2019.91001
44. Khalek MAA, Mahmoud GA, Shoukry EM, et al (2019) Adsorptive removal of nitrate ions from aqueous solution using modified biodegradable-based hydrogel. Desalination and Water Treatment 155:390–401. https://doi.org/10.5004/dwt.2019.24096
45. Khulbe KC, Matsuura T (2018) Removal of heavy metals and pollutants by membrane adsorption techniques. Applied Water Science 8:19. https://doi.org/10.1007/s13201-018-0661-6

46. Kozera-Sucharda B, Gworek B, Kondzielski I (2020) The simultaneous removal of zinc and cadmium from multicomponent aqueous solutions by their sorption onto selected natural and synthetic zeolites. Minerals 10:343. https://doi.org/10.3390/min10040343
47. Le QTN, Vivas EL, Cho K (2021) Oxalated blast-furnace slag for the removal of Cobalt(II) ions from aqueous solutions. Journal of Industrial and Engineering Chemistry 95:57–65. https://doi.org/10.1016/J.JIEC.2020.12.003
48. Limiju X (2017) APHA standard methods 23rd edition pdf
49. Liu SY, Gao J, Yang YJ, et al (2010) Adsorption intrinsic kinetics and isotherms of lead ions on steel slag. Journal of Hazardous Materials 173:558–562. https://doi.org/10.1016/j.jhazmat.2009.08.122
50. Lopes ECN, dos Anjos FSC, Vieira EFS, Cestari AR (2003) An alternative Avrami equation to evaluate kinetic parameters of the interaction of Hg(II) with thin chitosan membranes. Journal of Colloid and Interface Science 263:542–547. https://doi.org/10.1016/S0021-9797(03)00326-6
51. Maged A, Ismael IS, Kharbish S, et al (2020) Enhanced interlayer trapping of Pb(II) ions within kaolinite layers: intercalation, characterization, and sorption studies. Environmental Science and Pollution Research 27:1870–1887. https://doi.org/10.1007/s11356-019-06845-w
52. Mahmoud GA, Abdel Khalek MA, Shoukry EM, et al (2019) Removal of phosphate ions from wastewater by treated hydrogel based on chitosan. Egyptian Journal of Chemistry 62:1537–1549. https://doi.org/10.21608/EJCHEM.2019.9627.1646
53. Medina TJ, Arredondo SP, Corral R, et al (2020) Microstructure and pb2+ adsorption properties of blast furnace slag and fly ash based geopolymers. Minerals 10:1–17. https://doi.org/10.3390/min10090808
54. Mercado-Borrayo BM, Contreras R, Sánchez A, et al (2020) Optimisation of the removal conditions for heavy metals from water: A comparison between steel furnace slag and CeO2 nanoparticles. Arabian Journal of Chemistry 13:1712–1719. https://doi.org/10.1016/j.arabjc.2018.01.008
55. Mostafa NY, El-Hemaly SAS, Al-Wakeel EI, et al (2001) Characterization and evaluation of the hydraulic activity of water-cooled slag and air-cooled slag. Cement and Concrete Research 31:899–904. https://doi.org/10.1016/S0008-8846(01)00497-5
56. Narayanan S, Tamizhdurai P, Mangesh VL, et al (2020) Recent advances in the synthesis and applications of mordenite zeolite - review. RSC Advances 11:250–267
57. Nasuha N, Ismail S, Hameed BH (2016) Activated electric arc furnace slag as an efficient and reusable heterogeneous Fenton-like catalyst for the degradation of Reactive Black 5. Journal of the Taiwan Institute of Chemical Engineers 67:235–243. https://doi.org/10.1016/j.jtice.2016.07.023
58. Ostrovskii VE (1989) Mechanism of ammonia synthesis over iron catalysts in the equilibrium region. Theoretical and Experimental Chemistry 25:193–201. https://doi.org/10.1007/BF01135010
59. Petrakis E, Komnitsas K (2019) Effect of Energy Input in a Ball Mill on Dimensional Properties of Grinding Products. Mining, Metallurgy and Exploration 36:803–816. https://doi.org/10.1007/s42461-019-0066-6
60. Plaza L, Castellote M, Nevshupa R, Jimenez-Relinque E (2021) High-capacity adsorbents from stainless steel slag for the control of dye pollutants in water. Environmental Science and Pollution Research 2021 28:19 28:23896–23910. https://doi.org/10.1007/S11356-020-12174-0

61. Riley AL, Mayes WM (2015) Long-term evolution of highly alkaline steel slag drainage waters. Environmental Monitoring and Assessment 2015 187:7 187:1–16. https://doi.org/10.1007/S10661-015-4693-1
62. Rukayat OO, Usman MF, Elizabeth OM, et al (2021) Kinetic Adsorption of Heavy Metal (Copper) On Rubber (Hevea Brasiliensis) Leaf Powder. South African Journal of Chemical Engineering 37:74–80. https://doi.org/10.1016/j.sajce.2021.04.004
63. Saleem J, Shahid U Bin, Hijab M, et al (2019) Production and applications of activated carbons as adsorbents from olive stones. Biomass Conversion and Biorefinery 9:775–802
64. Sall ML, Diaw AKD, Gningue-Sall D, et al (2020) Toxic heavy metals: impact on the environment and human health, and treatment with conducting organic polymers, a review. Environmental Science and Pollution Research 27:29927–29942
65. Sen Gupta S, Bhattacharyya KG (2014) Adsorption of metal ions by clays and inorganic solids. RSC Advances 4:28537–28586
66. Shehab A, Abdelbasir SM, Khalek MAA, Soliman MH (2019) Dye Removal from Aqueous Solution by Regenerated Spent Bleaching Earth. International Journal of Chemical, Materials and Biomolecular Sciences 333–340
67. Sundhararasu E, Tuomikoski S, Runtti H, et al (2021) Alkali-Activated Adsorbents from Slags: Column Adsorption and Regeneration Study for Nickel(II) Removal. ChemEngineering 2021, Vol 5, Page 13 5:13. https://doi.org/10.3390/CHEMENGINEERING5010013
68. Tsai W-T, Chen H-R (2013) Adsorption kinetics of herbicide paraquat in aqueous solution onto a low-cost adsorbent, swine-manure-derived biochar. International Journal of Environmental Science and Technology 10:1349–1356. https://doi.org/10.1007/s13762-012-0174-z
69. Tsutsumi T, Nishimoto S, Kameshima Y, Miyake M (2014) Hydrothermal preparation of tobermorite from blast furnace slag for Cs+ and Sr2+ sorption. Journal of Hazardous Materials 266:174–181. https://doi.org/10.1016/J.JHAZMAT.2013.12.024
70. Vaghetti JCP, Lima EC, Royer B, et al (2009) Pecan nutshell as biosorbent to remove Cu(II), Mn(II) and Pb(II) from aqueous solutions. Journal of Hazardous Materials 162:270–280. https://doi.org/10.1016/j.jhazmat.2008.05.039
71. Visa M (2016) Synthesis and characterization of new zeolite materials obtained from fly ash for heavy metals removal in advanced wastewater treatment. Powder Technology 294:338–347. https://doi.org/10.1016/j.powtec.2016.02.019
72. Wang F, Lu X, Li XY (2016) Selective removals of heavy metals (Pb2+, Cu2+, and Cd2+) from wastewater by gelation with alginate for effective metal recovery. Journal of Hazardous Materials 308:75–83. https://doi.org/10.1016/j.jhazmat.2016.01.021
73. Wang Y, Li H, Cui S, Wei Q (2021) Adsorption Behavior of Lead Ions from Wastewater on Pristine and Aminopropyl-Modified Blast Furnace Slag. Water 2021, Vol 13, Page 2735 13:2735. https://doi.org/10.3390/W13192735
74. Xiong J, He Z, Mahmood Q, et al (2008) Phosphate removal from solution using steel slag through magnetic separation. Journal of Hazardous Materials 152:211–215. https://doi.org/10.1016/j.jhazmat.2007.06.103

75. Xue Y, Hou H, Zhu S (2009) Adsorption removal of reactive dyes from aqueous solution by modified basic oxygen furnace slag: Isotherm and kinetic study. Chemical Engineering Journal 147:272–279. https://doi.org/10.1016/j.cej.2008.07.017
76. Yang L, Wen T, Wang L, et al (2019) The stability of the compounds formed in the process of removal Pb(II), Cu(II) and Cd(II) by steelmaking slag in an acidic aqueous solution. Journal of Environmental Management 231:41–48. https://doi.org/10.1016/J.JENVMAN.2018.10.028
77. Yildirim IZ, Prezzi M (2011) Chemical, mineralogical, and morphological properties of steel slag. Advances in Civil Engineering 2011:. https://doi.org/10.1155/2011/463638
78. Zare EN, Lakouraj MM, Masoumi M (2018) Efficient removal of pb (II) and Cd (II) from water by cross-linked poly (N-vinylpyrrolidone-co-maleic anhydride)@eggshell/Fe3 O4 environmentally friendly nano composite. Desalination and Water Treatment 106:209–219. https://doi.org/10.5004/dwt.2018.22104
79. Zare EN, Lakouraj MM, Ramezani A (2016) Efficient sorption of Pb(II) from an aqueous solution using a poly(aniline-co-3-aminobenzoic acid)-based magnetic core-shell nanocomposite. New Journal of Chemistry 40:2521–2529. https://doi.org/10.1039/c5nj02880a
80. Zhan X, Xiao L, Liang B (2019) Removal of Pb(II) from Acid Mine Drainage with Bentonite-Steel Slag Composite Particles. Sustainability 2019, Vol 11, Page 4476 11:4476. https://doi.org/10.3390/SU11164476

Figures

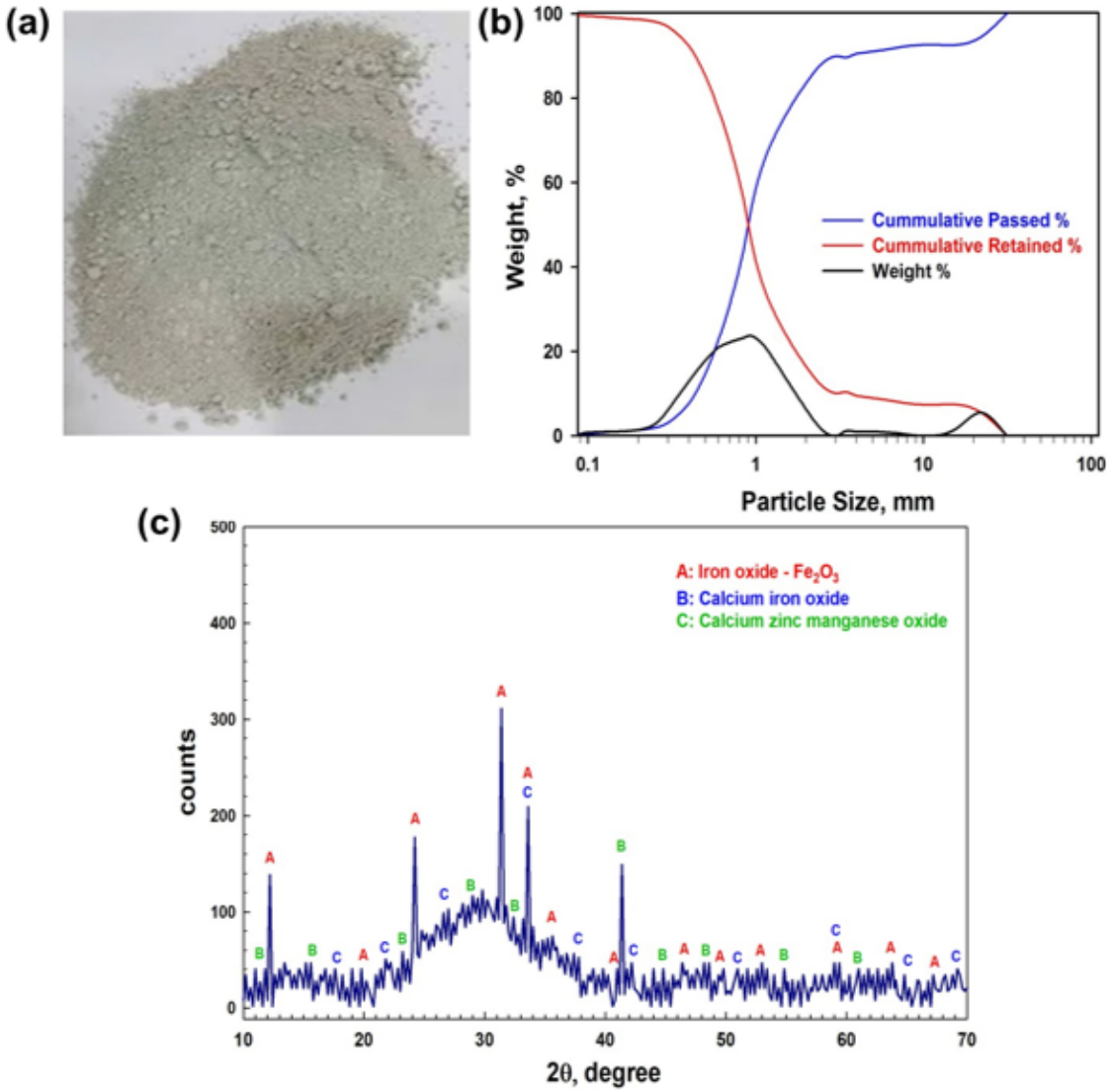

Figure 1

(a) A photo of the ground BFS (b) **s**ize analysis of the ground sample, weight, cumulative passed and retained, (c) XRD pattern of BFS.

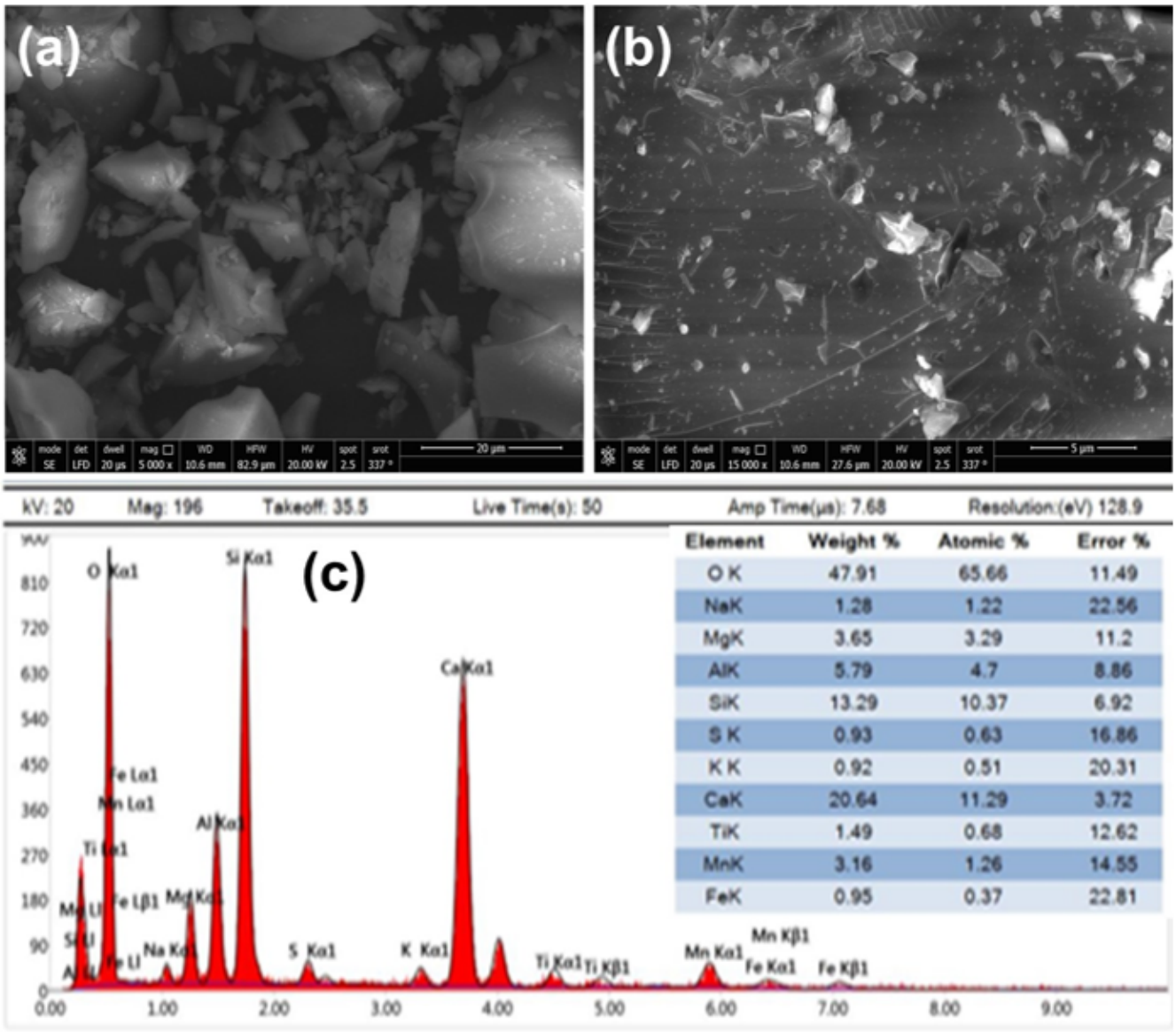

Figure 2

SEM images: (a) 20 µm, (b) 5 µm, and (c) EDX analysis of BFS.

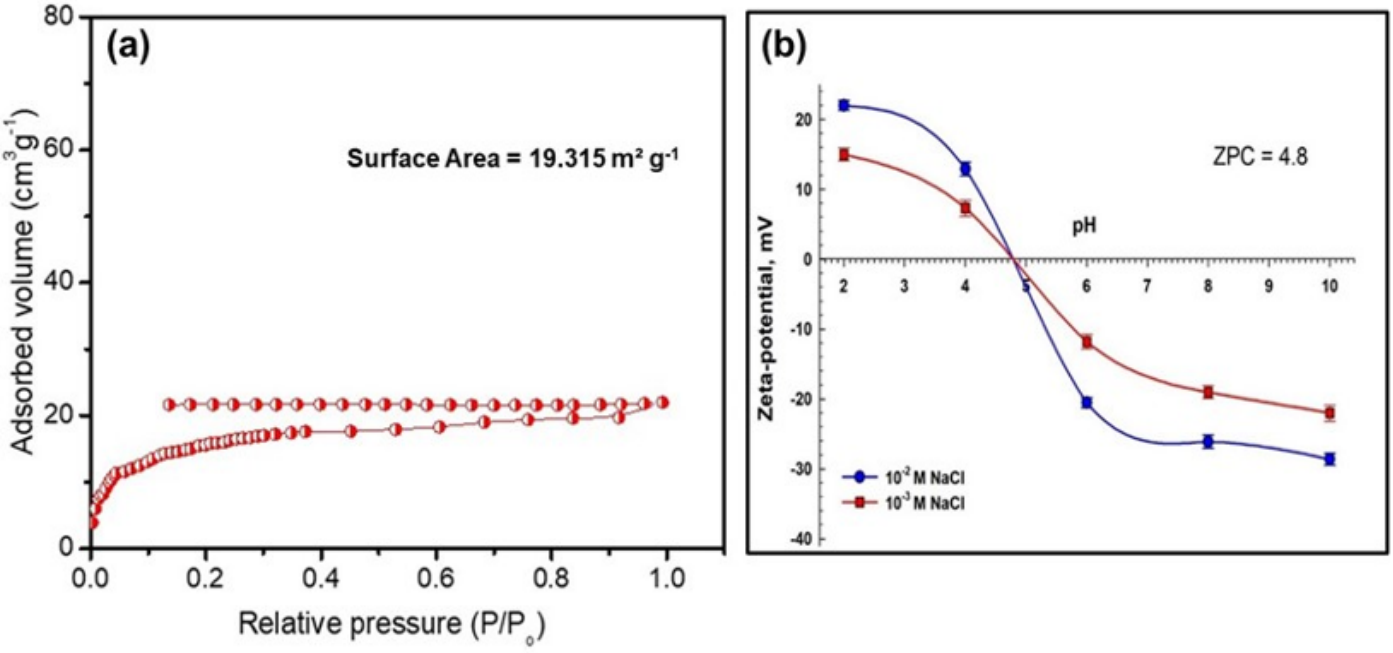

Figure 3

(a) N_2 adsorption isotherm and (b) Zeta potential of the BFS.

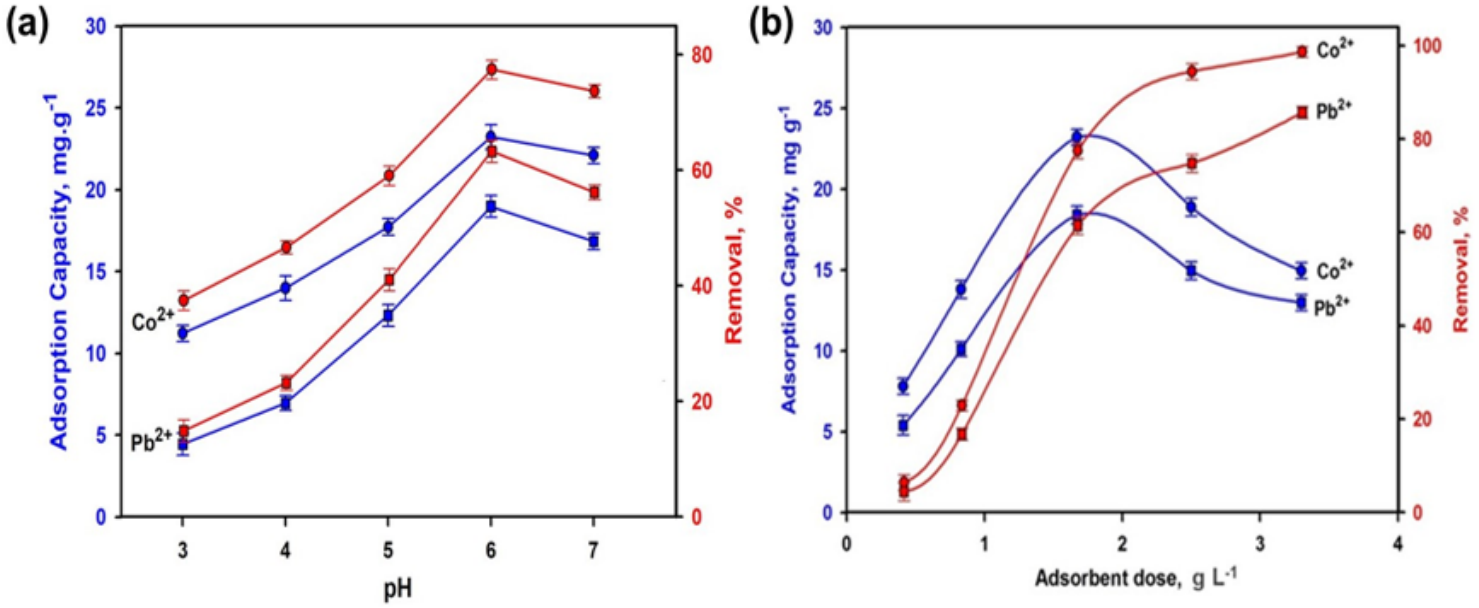

Figure 4

(a) Effect of pH (initial concentration: 50 mg L^{-1}, adsorbent doze: 1.67g L^{-1}, contact time: 60 min. at room temperature), (b) Effect of slag dose (initial concentration: 50 mg L^{-1}, contact time: 60 min. at room temperature) on the removal efficiency and adsorption capacity of slag.

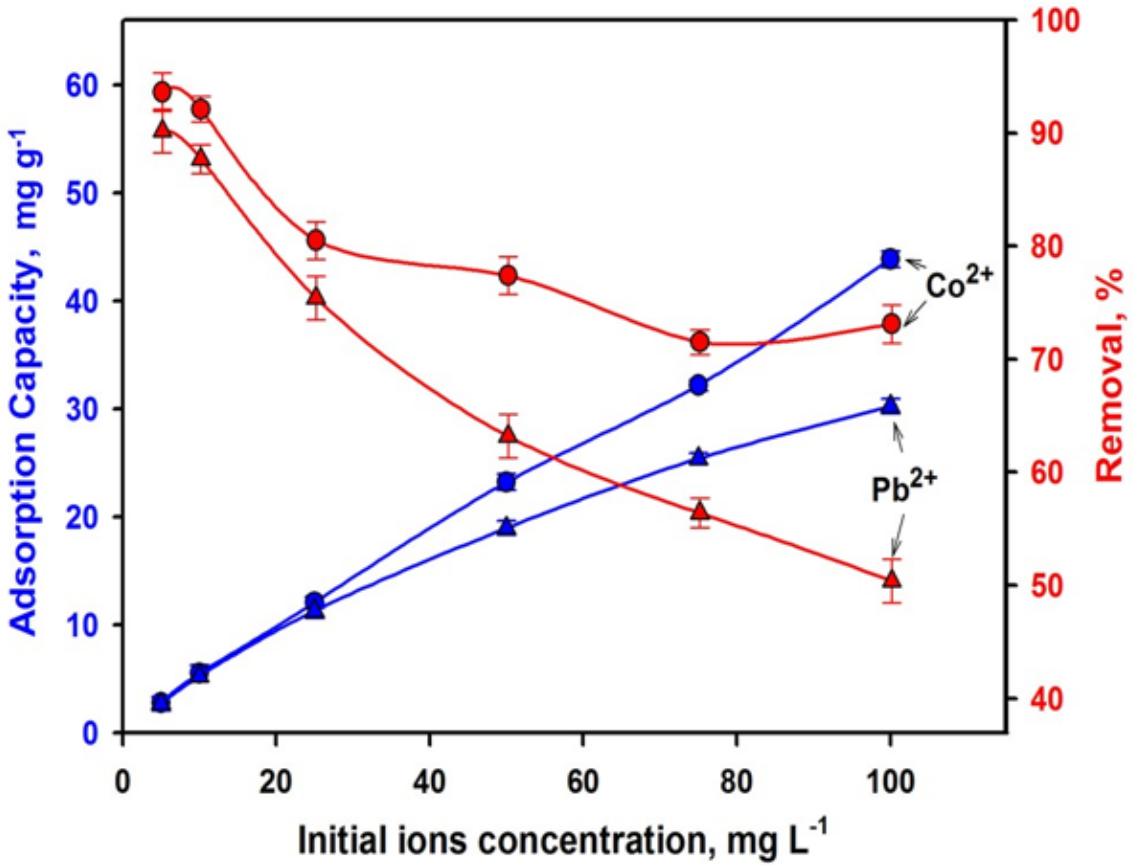

Figure 5

Effect of initial concentration on the removal efficiency and adsorption capacity (adsorbent doze: 1.67g L^{-1}, contact time: 60 min., at solution pH: 6 and room temperature).

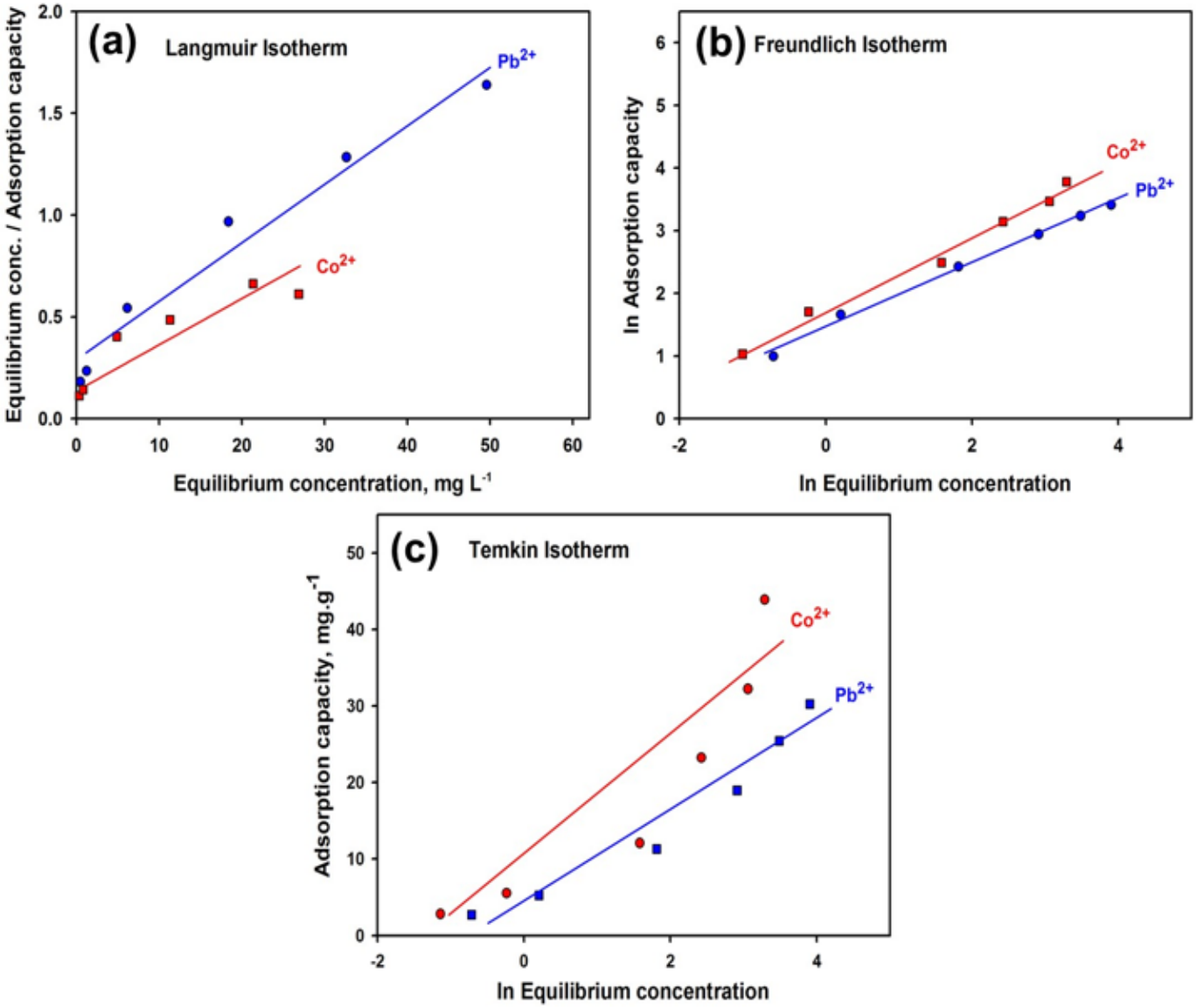

Figure 6

Plotting results according to (a) Langmuir, (b) Freundlich, and (c) Temkin isotherms ((initial concentration: 50 mg L^{-1}, contact time: 60 min. at room temperature).

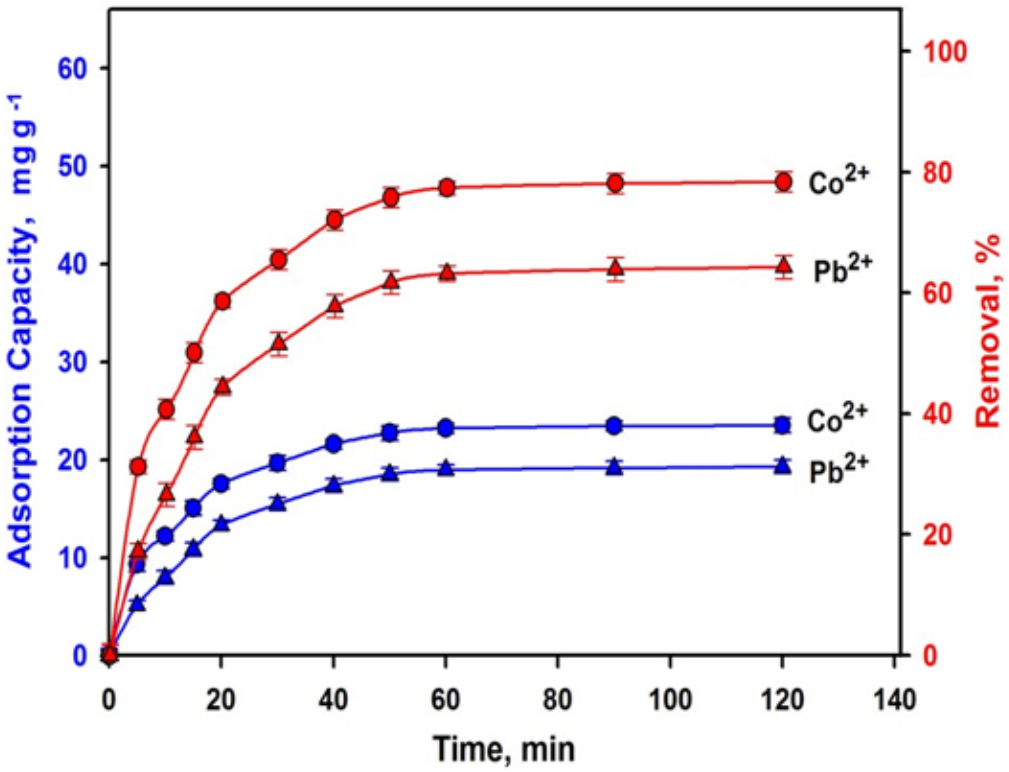

Figure 7

Effect of conditioning time on the removal efficiency and adsorption capacity of slag (initial concentration: 50 mg L^{-1}, adsorbent doze: 1.67g $^{-1}$, solution pH:6 at room temperature).

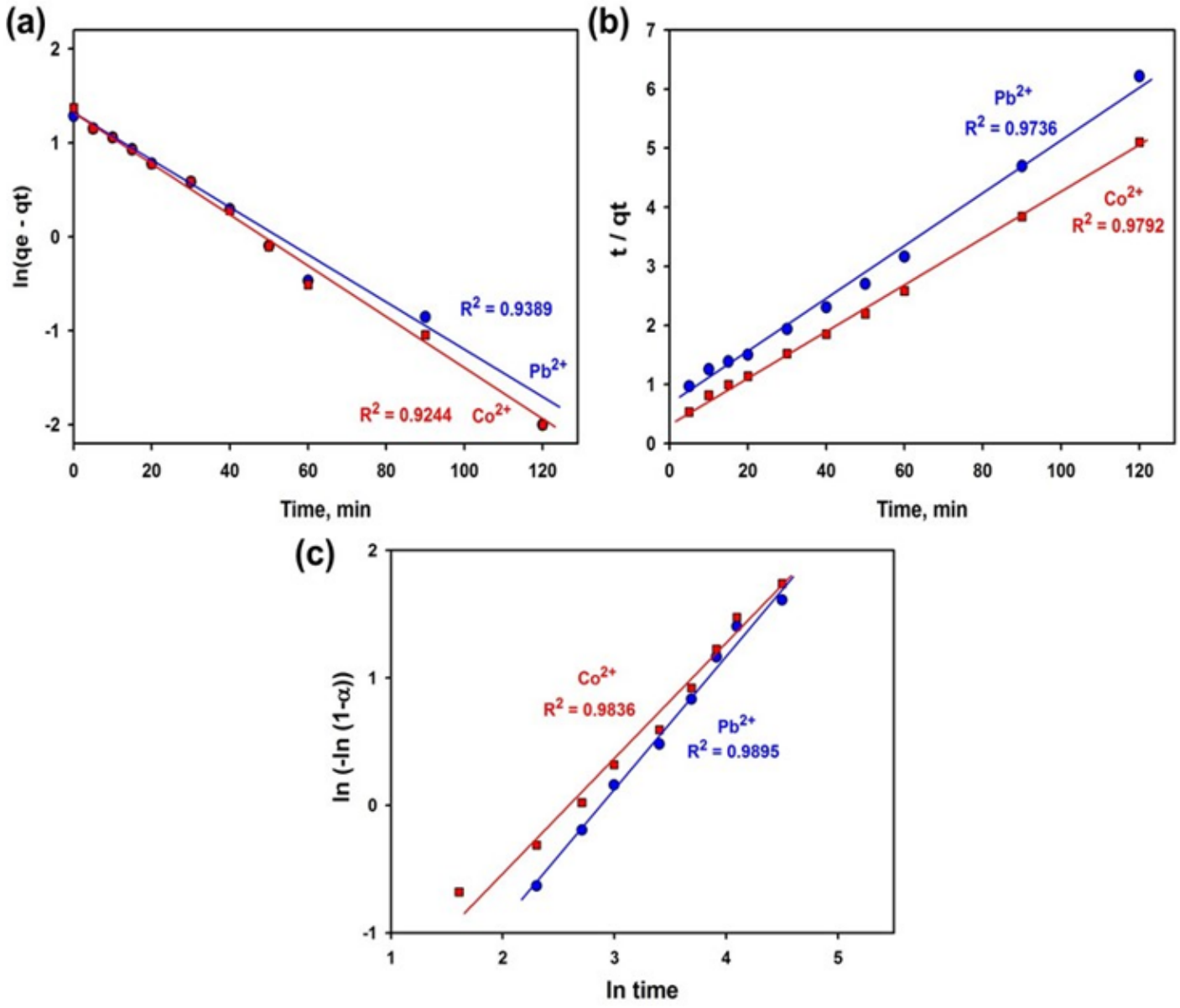

Figure 8

Plotting results according to the three kinetics models (a) pseudo-first-order; (b) pseudo-second-order; and (c) Avrami.

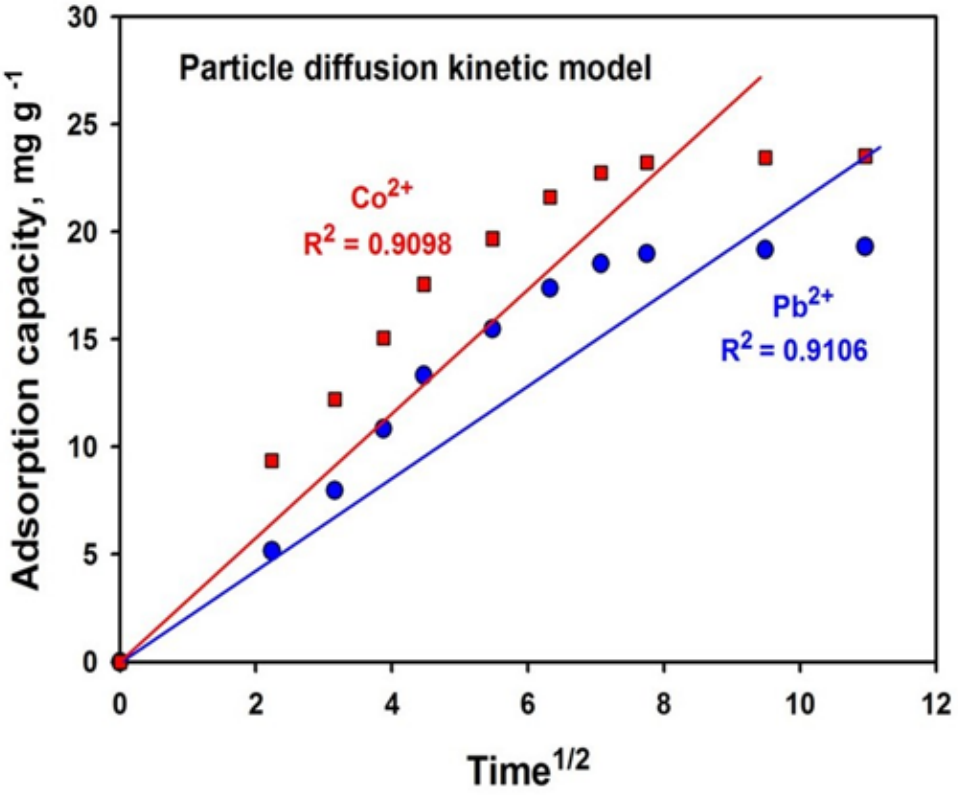

Figure 9

Plot of particle diffusion kinetic model.

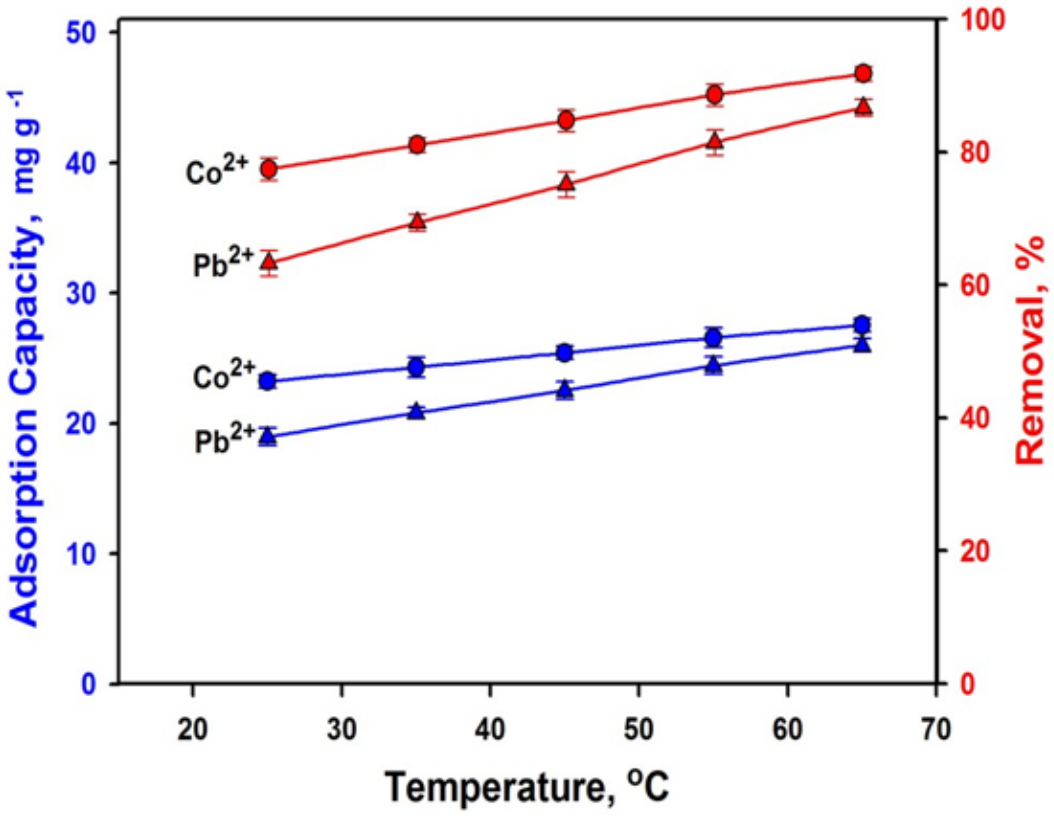

Figure 10

Effect of temperature on the removal efficiency of Co^{2+} and Pb^{2+} ions and adsorption capacity of BFS.

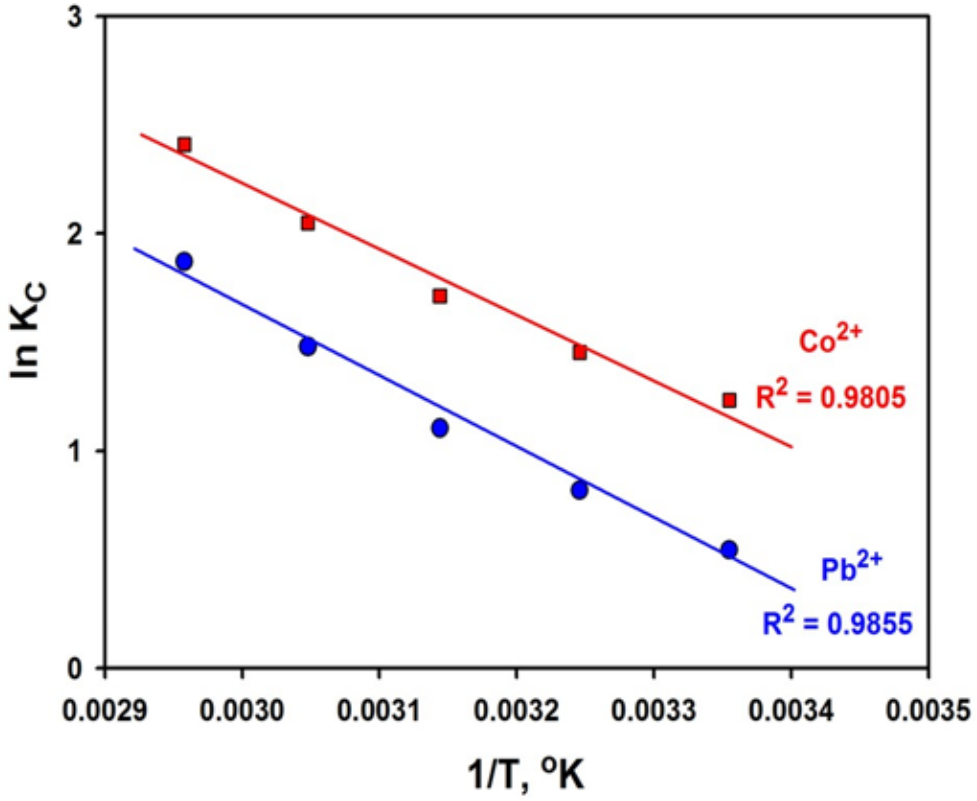

Figure 11

Plot of lnk_c versus 1/T.

Supplementary Files

This is a list of supplementary files associated with this preprint. Click to download.

- Graphicalabstract.tif
- Slagsupplemental.docx